Tribology Letters (2025) 73:106
https://doi.org/10.1007/s11249-025-02046-4

ORIGINAL PAPER

The Effect of Hardness and Surface Roughness of Elastomer on Friction Between Shoe Soles and Particle-Contaminated Floors

Michal Žůrek[1] · David Markusík[2,4] · David Rebenda[1,3] · Lukáš Kalina[2] · Martin Hartl[1] · Martin Vrbka[1]

Received: 15 May 2025 / Accepted: 13 July 2025 / Published online: 19 July 2025

Abstract

Nearly one third of workplace injuries results from slip- and trip-induced falls. Solid particles are among the most common floor contaminants in both occupational and outdoor environments, reducing shoe–floor friction and increasing slip risk. This study investigates how rubber hardness and surface roughness affect the frictional behaviour of shoe soles on smooth, particle-contaminated floors. Coefficient of friction (COF) measurements and post-test surface wear analyses were conducted using nitrile rubbers with hardness between 57.9 and 84.0 ShA and varied surface roughness. Samples were slid against smooth epoxy flooring in a pin-on-plate test simulating the heel-strike phase of walking. The floor was either clean or uniformly covered with corundum particles (40–50 µm, 120–140 µm, or 280–315 µm). On clean floors, increasing rubber hardness and roughness significantly decreased COF ($p < 0.0001$) due to reduced real contact area. Under contaminated conditions, softer and rougher rubbers yielded higher COF values ($p < 0.0001$). Higher COF correlated with greater floor wear, showing long scratches and grooves, suggesting slip occurs mainly at the particle–floor interface. Rubber hardness and surface roughness primarily influence the strength of the particle–elastomer interface; greater particle–elastomer strength suppresses particle rolling and thereby leads to an increase in COF. These findings indicate that, on particle-contaminated smooth floors, slip resistance is governed more by particle–floor interactions than by rubber adhesion. Increasing outsole roughness and reducing hardness can help mitigate the adverse effects of particle rolling within the contact area and improve the frictional performance of the outsole.

✉ Michal Žůrek
Michal.Zurek1@vut.cz

[1] Biotribology Research Group, Faculty of Mechanical Engineering, Brno University of Technology, Technická 2896/2, 616 69 Brno, Czech Republic

[2] Institute of Materials Science, Faculty of Chemistry, Brno University of Technology, Purkyňova 464/118, 612 00 Brno, Czech Republic

[3] Centre of Polymer Systems, University Institute, Tomas Bata University in Zlin, Třída Tomáše Bati 5678, 760 01 Zlín, Czech Republic

[4] Institute of Physics of Materials, Czech Academy of Sciences, Žižkova 22, 616 00 Brno, Czech Republic

Graphical Abstract

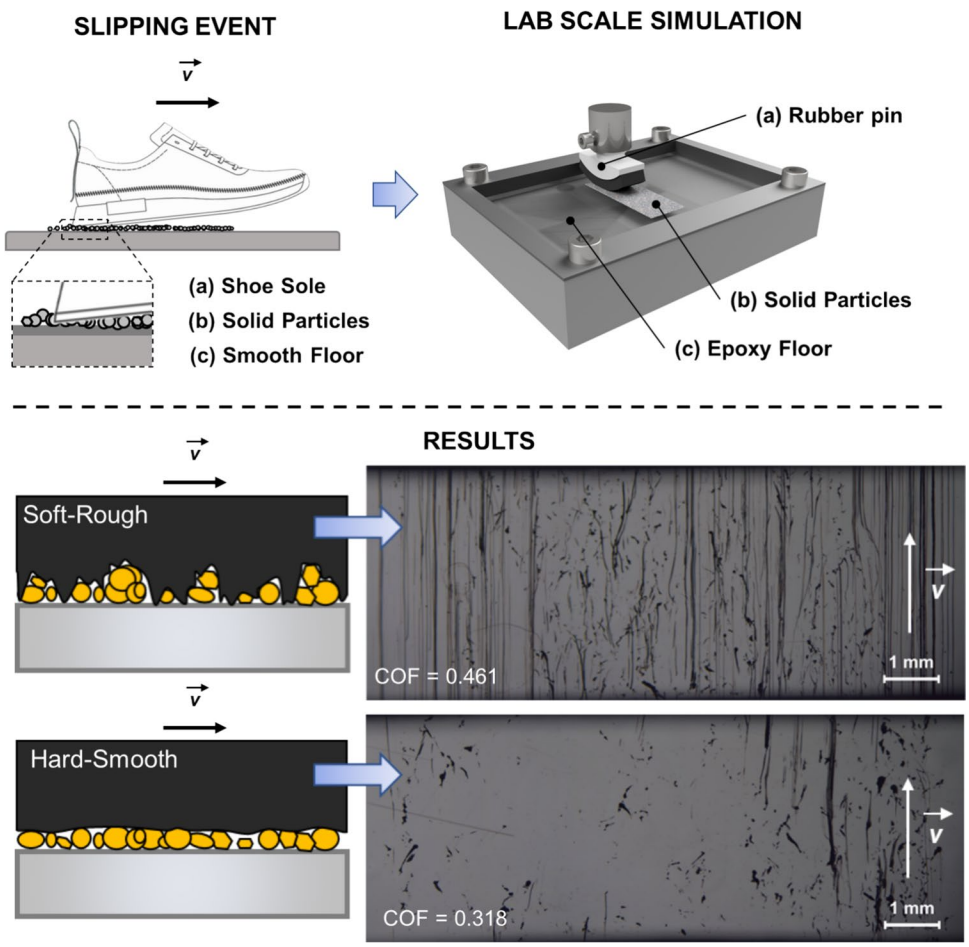

Keywords Slip resistance · Particle contamination · Rubber friction · Surface wear · Workplace safety

1 Introduction

Slips and trips are a major cause of non-fatal workplace injuries, accounting for 32% of cases in the United Kingdom, 25% in Japan, and 18% in the United States [1–3]. Nearly half of all fall-related injuries are associated with unexpected slipping [4], and almost 80% of slips result from an inadequate floor surface or sole material [5]. Slip risk is evaluated by comparing the required coefficient of friction (RCOF)—the friction needed by a pedestrian to perform movement—with the available coefficient of friction (ACOF) at the shoe/surface interface in a given environment. If the available friction exceeds the required friction, slipping does not occur [6]. Slipping prevention can be based on two approaches: recommendations aimed at adjusting pedestrian movement to deteriorated environmental conditions, thereby ensuring a lower RCOF, or the development and implementation of improved footwear and flooring materials in workplaces and public spaces, leading to an increased ACOF.

Compared to clean and dry floor surfaces, contaminated surfaces pose a higher risk of slipping. The presence of a contaminant prevents direct contact between the shoe sole and the ground, suppressing adhesion and consequently lowering the coefficient of friction (COF) between the two surfaces. Mechanisms of slipping at the shoe-floor interface are markedly different for liquid and solid type of contamination. For liquid contamination, the contaminant film thickness is the key parameter that defines the lubrication regime. Pedestrian slips on liquid contaminated floors usually operate in boundary or mixed regime, but do not reach the hydrodynamic regime [7].

Li et al. [8] observed that solid particles at the shoe-floor interface can reduce the COF more than the presence of a liquid. The primary slip mechanisms in particle-contaminated interfaces include sliding, shearing, and rolling, with

key influencing factors being floor surface roughness, particle size, and particle shape [9]. On smooth surfaces, slipping is mainly driven by sliding, whereas on rougher surfaces, such as asphalt pavement, shearing and rolling dominate [10].

Research on road surfaces contaminated by solid particles has shown that fine particles become embedded in surface microtexture, prolonging friction reduction, whereas coarse particles are expelled more quickly, allowing for faster friction recovery [11]. Additionally, the material composition of particles influences slip risk. Hard particles, such as quartz, exhibit rolling and scratching behaviour, while soft materials like clay adhere to surfaces, leading to prolonged contamination and lower friction [12].

Coverage fraction also plays a critical role in slipping. Friction reduction follows a Stribeck-like pattern, with the steepest decline occurring at intermediate coverage levels (10–45%) before stabilizing at higher fractions [13].

The effects of material properties of shoe soles such as hardness and roughness have been studied mostly for dry, uncontaminated surfaces and surfaces contaminated with liquids [14–16]. However, research on the influence of these factors in particle-contaminated contact remains limited. Li et al. [17] reported mixed effects of elastomer hardness on COF. When the surface was contaminated with particles, a decrease in COF was observed for a hard Neolite material (93 ShA), whereas a soft EVA material (45 ShA) exhibited an increase in COF in the presence of particles.

This study aims to clarify the impact of sole material hardness and roughness on COF when in contact with a smooth floor surface under solid contamination. Based on previous findings, it is expected that increased rubber roughness will promote direct contact between rubber asperities and the floor, thereby increase the COF. This effect is anticipated to be more pronounced for harder rubber materials, as their asperities undergo less deformation under load and are better able to displace particles, establishing direct contact with the floor. Conversely, for smooth soles, increasing hardness is expected to reduce particle penetration into the rubber surface, leading to higher separation between the sole and the floor and consequently lowering COF [18].

2 Materials and Methods

An experimental matrix was designed to test the hypotheses about friction of rubber on a smooth epoxy surface. The experiments cover the range of rubber surface roughness achievable by common grinding methods (Ra: 0.5–65 µm) and hardness within the range used for manufacturing shoe outsoles (57.9–84.0 ShA). Two main datasets were created. The first dataset, corresponding to surfaces contaminated with solid particles, was based on three levels of rubber surface roughness, three particle size fractions, and four levels of rubber hardness.

Measurements for each combination of conditions were repeated five times, resulting in a total of 180 measurements for contaminated surfaces. The second dataset, used for comparison with a clean epoxy surface, also included three rubber surface roughness levels and four rubber hardness levels, with five repetitions for each combination. This resulted in a total of 60 measurements for clean epoxy surfaces. The response variables were the COF and the slope of COF.

2.1 Materials

2.1.1 Rubber Specimens

Rubber sheets with a thickness of 4 mm, based on nitrile rubber (NBR), were supplied by GUMEX, spol. s.r.o. (Brno, Czech Republic). The hardness of the rubber sheets was determined according to the EN ISO 868:2003 standard [19] using a durometer, yielding values of 57.9 ± 0.6 ShA, 67.4 ± 1.4 ShA, 74.1 ± 1.4 ShA, and 84.0 ± 0.6 ShA. The surface of the plates was unidirectionally abraded to the desired roughness using abrasive paper of different grit sizes (P24 and P60) (Fig. 1). Rubber samples with varying surface roughness were glued onto PLA pins with a radius of curvature $R = 20$ mm, such that the grooving was oriented perpendicular to the direction of sliding. The curvature ensured that, during sliding, new particles could continuously enter the contact area.

2.1.2 Epoxy Flooring

A two-component epoxy resin, based on 2,2′-[(1-methylethylidene)bis(4,1-phenyleneoxymethylene)]bisoxirane and 3-aminomethyl-3,5,5-trimethylcyclohexylamine with 4,4′-isopropylidenediphenol (purchased from EPODEX GmbH), was cast into 3D-printed PLA moulds to form a layer with a final thickness of 3–5 mm. After complete curing, its hardness was measured according to EN ISO 868:2003 standard [19] at 82.4 ± 0.4 ShD.

2.1.3 Solid Particles

Corundum particles (Al_2O_3) were sieved into three distinct grain size fractions: 40–50 µm, 120–140 µm, and 280–315 µm. The particle shape was subsequently evaluated using SEM imaging.

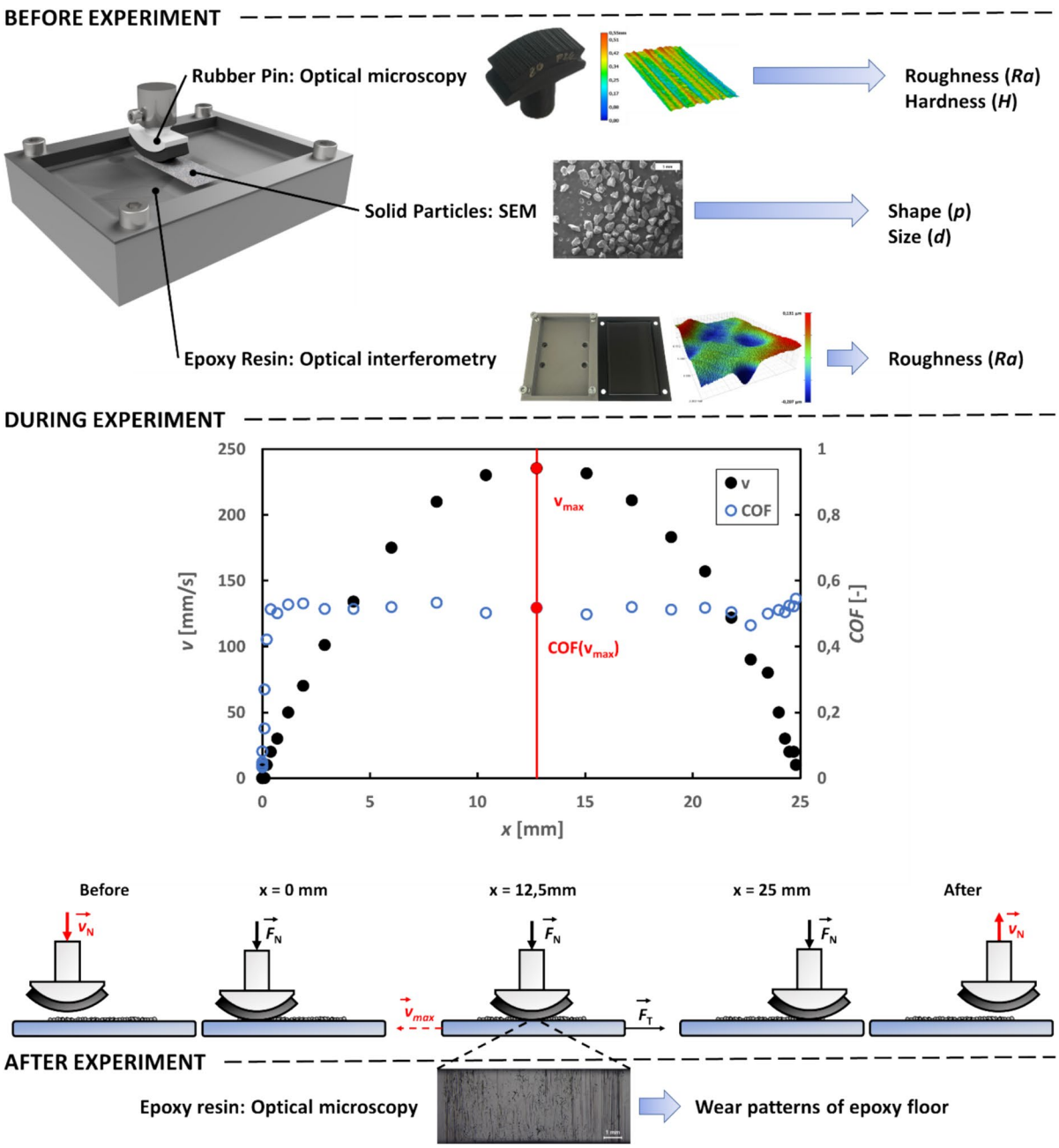

Fig. 1 Rubber surfaces prepared by unidirectional sandpaper grinding: no gringing **a**, sandpaper P60 **b**, sandpaper P24 **c**

2.2 Methods

2.2.1 Coefficient of Friction

A commercial device UMT Tribolab Bruker was used to measure COF in a pin-on-plate test configuration. The rubber pin was mounted in the upper module with its cylindrical axis oriented perpendicular to the sliding direction (Fig. 2). The epoxy plate was fixed in the lower reciprocating module. Using a custom-made frame, the epoxy surface was uniformly covered with 0.3 g of contaminant particles along the entire sliding track.

The pin was initially loaded at a vertical speed of 0.5 mm/s until a normal force of 8 N (pretouch) was reached, and then pressed further at 0.1 mm/s to a final normal force of 10 N (touch). Depending on the pin hardness, the applied load resulted in an apparent contact area ranging from 0.21 cm^2 to 0.42 cm^2, the estimation was made using classical Hertz contact model. The corresponding predicted

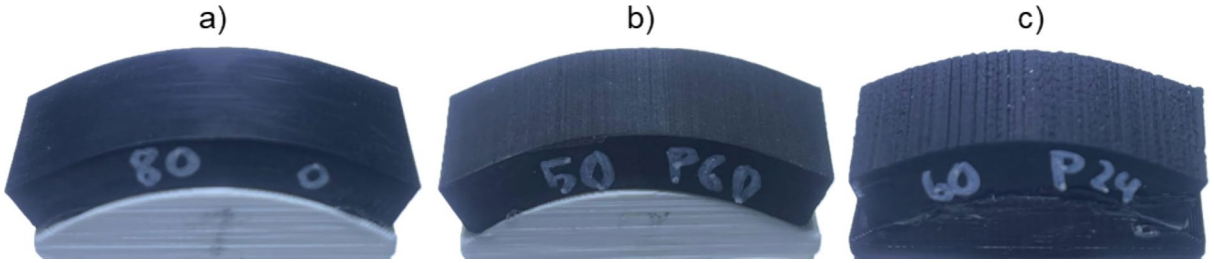

Fig. 2 General scheme of materials and methods used in the present study

contact pressure (238–484 kPa) represents biomechanically relevant conditions [20].

The motion of the reciprocating module simulated the slipping event of a person stepping onto a floor surface. The maximum sliding velocity during all measurements was $v_{max} = 235.3 \pm 0.6$ mm/s, which is close to the upper limit of the heel-strike velocity range observed in human walking (0.14–0.24 m/s) [21]. The total sliding distance was 25 mm, corresponding to the maximum stroke length of the reciprocating module in the employed device.

Each measurement was performed on a new track of the epoxy plate to ensure that subsequent measurements were not influenced by surface scratches caused by corundum particles. Figure 2 shows the evolution of the COF and sliding velocity during a single measurement. For each combination of input conditions (Ra, H, and d), the coefficient of friction at maximum velocity ($COFv_{max}$) was calculated as the average of five repeated measurements.

Additionally, the slope of the COF as a function of sliding distance x, during the portion of the test where the velocity exceeded 130 mm/s, was evaluated to gain further insight into the frictional behaviour during sliding (Fig. 3).

2.2.2 Surface Roughness

The surfaces of all rubber pins were scanned using a KEYENCE VHX-7000 digital microscope at a magnification of 100×. Surface roughness parameters were evaluated as the average of five line-profile sections oriented perpendicular to the grooves formed during the grinding process. The cut-off wavelength (λ_c) was set to 0.8 mm for smooth rubber surfaces and 2.5 mm for roughened surfaces, thereby removing waviness and curvature from the surface profile.

The surface of the epoxy plate was scanned using a Bruker Contour GT-X optical profilometer at a magnification of 2.75× (using a 5× objective with a 0.55× reduction). The roughness of the smooth surface prior to the friction testing was assessed over an area of 3.74 mm^2, following tilt correction using a plane-fit method. The measurement was carried out on one epoxy sample with the aim of providing an approximate roughness value of the cast epoxy surface, to avoid relying solely on the qualitative descriptor "smooth" and to enable at least a basic quantitative characterization of the initial surface condition.

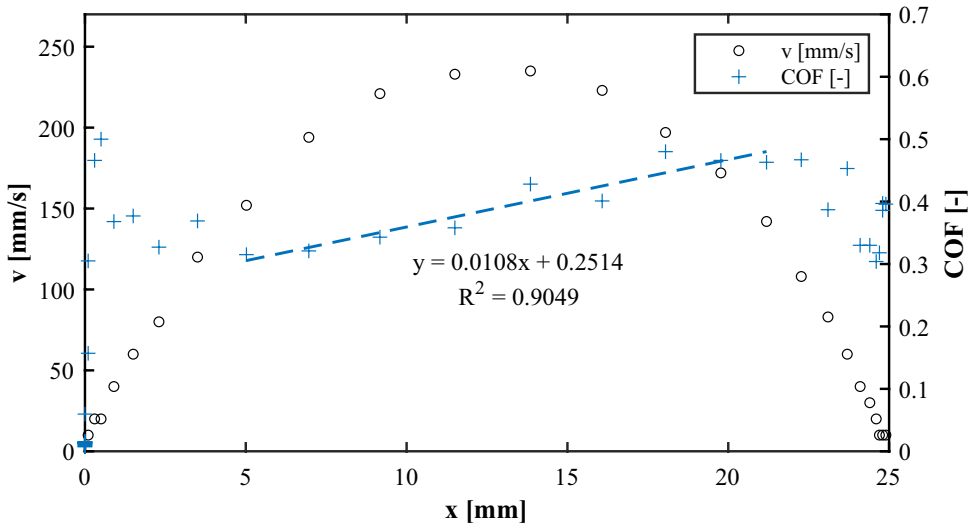

Fig. 3 COF behaviour during sliding for hard rough rubber pin (84.0 ShA, P24) with contaminant particles sized 280–315 µm

2.2.3 Analysis of Epoxy Flooring Wear

The worn epoxy surfaces were examined after the friction experiments using rubber pins with the lowest and highest hardness and roughness values, employing an optical microscope at 1.5 × magnification equipped with a digital camera. The wear patterns were then assessed from the images taken at the location corresponding to the recorded $COFv_{max}$.

2.2.4 Analysis of Solid Particles

To evaluate the shape of particles in different size fractions, SEM images were taken at magnifications of 50 ×, 100 ×, and 200 × using a Zeiss EVO LS 10 scanning electron microscope. Particle shape was analysed from 2D images using ImageJ software. The primary shape parameter of interest was particle roundness, calculated from the perimeter and area of individual particles (Eq. 1).

$$F = \frac{4\pi A}{p^2}, \tag{1}$$

where F is the roundness of the particle, A is the area, and p is the perimeter of the particle in a 2D SEM image. The roundness value ranges from 0 (a straight line) to 1 (a perfect circle).

2.3 Data Analysis

After performing five repeated measurements for all experimental conditions, we obtained 240 values of COF and 240 values of the slope of COF. A Dixon's Q test ($p < 0.1$) was performed separately for each response variable to identify statistically significant outliers within each measurement group. This resulted in two datasets cleaned of outliers, one for COF and one for the slope of COF.

Each dataset was then divided into two subsets: one for clean and one for particle-contaminated conditions, as the effects of sole material on COF and its slope are expected to differ fundamentally between these two surface conditions.

ANOVA was performed independently for COF and for the slope of COF, and separately for clean and contaminated surfaces, to evaluate the statistical significance of the effects of rubber hardness, rubber surface roughness, and—where applicable—particle size.

Table 1 Particle Roundness Values Across Size Fractions

Particle size	40–50 µm	120–140 µm	280–315 µm
F [−]	0.56 ± 0.17	0.51 ± 0.16	0.70 ± 0.15

3 Results

3.1 Shape of Solid Particles

The roundness (F) of individual particle size fractions is presented in Table 1. Corundum particles in the size ranges of 40–50 µm and 120–140 µm exhibit relatively similar shapes, whereas the roundness of particles in the 280–315 µm size range is significantly higher.

3.2 Roughness of Contacting Surfaces

The surface roughness of rubber achievable through sandpaper grinding is strongly influenced by the material properties of the rubber itself. The roughness values of the rubber pins used in this study are summarized in Table 2. The surface roughness of the smooth rubber corresponds approximately to the texture of the mould in which the plates were vulcanized. Increasing the sandpaper grit size resulted in higher surface roughness of the ground elastomer. The heterogeneous nature of coarse sandpaper also caused greater variability in surface roughness across the ground area.

The surface roughness (S_a) of the epoxy plate was determined to be 32 nm, which was considered smooth relative to the particle sizes used and the roughness of the rubber surfaces.

3.3 Coefficient of Friction

3.3.1 Clean Surface

On the clean epoxy surface, both the hardness and surface roughness of the rubber pin have a significant effect on the COF ($p < 0.0001$). The highest COF value (2.216 ± 0.027) was observed for rubber with low hardness and low surface roughness (H = 57.9 ShA, Ra = 0.56 µm). In contrast, the lowest COF value (0.70 ± 0.03) was recorded for rubber with high hardness and high surface roughness (84.0 ShA, Ra = 33.78 µm) (Table 3).

Table 2 Values of roughness (Ra) and standard deviation of rubber pins

Surface		57.9 ShA	67.4 ShA	74.1 ShA	84.0 ShA
Smooth	Ra [µm]	0.56 ± 0.04	0.65 ± 0.01	0.56 ± 0.05	0.61 ± 0.05
P60		6.7 ± 0.5	6.5 ± 0.8	9.5 ± 0.9	10 ± 1
P24		41 ± 4	27 ± 8	51 ± 11	37 ± 10

Table 3 Mean values of COF and their standard deviations for measurements on clean surface

d [µm]	H [ShA]	Ra [µm]	Mean COF [−]	STD [−]
Clean surface	57.9	0.56	2.216	0.027
	57.9	7.23	1.384	0.042
	57.9	39.45	1.254	0.015
	67.4	0.65	1.838	0.066
	67.4	5.70	1.192	0.039
	67.4	28.33	1.022	0.025
	74.1	0.56	1.398	0.050
	74.1	8.95	0.938	0.032
	74.1	54.91	0.773	0.003
	84.0	0.61	0.996	0.013
	84.0	10.82	0.767	0.013
	84.0	33.78	0.699	0.027

Table 4 Mean values of COF and their standard deviations for measurements on surface contaminated with particles sized 40–50 µm

d [µm]	H [ShA]	Ra [µm]	Mean COF [−]	STD [−]
40–50	57.9	0.53	0.537	0.007
	57.9	6.94	0.542	0.024
	57.9	47.27	0.553	0.012
	67.4	0.63	0.471	0.017
	67.4	6.55	0.529	0.005
	67.4	18.47	0.552	0.011
	74.1	0.51	0.506	0.026
	74.1	10.52	0.524	0.022
	74.1	44.53	0.567	0.008
	84.0	0.54	0.463	0.010
	84.0	8.30	0.513	0.012
	84.0	52.10	0.563	0.024

Table 5 Mean values of COF and their standard deviations for measurements on surface contaminated with particles sized 120–140 µm

d [µm]	H [ShA]	Ra [µm]	Mean COF [−]	STD [−]
120–140	57.9	0.53	0.500	0.018
	57.9	6.62	0.513	0.014
	57.9	39.28	0.527	0.011
	67.4	0.65	0.440	0.012
	67.4	7.58	0.450	0.007
	67.4	38.10	0.557	0.025
	74.1	0.63	0.430	0.027
	74.1	8.51	0.460	0.017
	74.1	64.98	0.546	0.020
	84.0	0.61	0.435	0.026
	84.0	11.58	0.450	0.020
	84.0	32.12	0.517	0.006

Table 6 Mean values of COF and their standard deviations for measurements on surface contaminated with particles sized 280–315 µm

d [µm]	H [ShA]	Ra [µm]	Mean COF [−]	STD [−]
280–315	57.9	0.62	0.432	0.002
	57.9	5.98	0.418	0.037
	57.9	37.76	0.461	0.029
	67.4	0.66	0.385	0.057
	67.4	6.18	0.436	0.017
	67.4	23.42	0.425	0.029
	74.1	0.55	0.354	0.037
	74.1	10.03	0.369	0.060
	74.1	40.86	0.451	0.048
	84.0	0.67	0.318	0.042
	84.0	10.18	0.327	0.074
	84.0	31.71	0.439	0.017

3.3.2 Contaminated Surface

For particles in the size range of 40–50 µm, COF values lie within the interval of 0.463–0.567 (Table 4). For particles sized 120–140 µm, COF values range from 0.430 to 0.557 (Table 5), and for particles sized 280–315 µm, the COF interval is 0.318–0.461 (Table 6). A comparison of the COF ranges resulting from variations in elastomer hardness and surface roughness (Fig. 4a) shows that these parameters have the greatest influence in the uncontaminated shoe–floor contact, where the COF range is the widest. On surfaces contaminated with particles, the COF ranges are notably narrower compared to the clean surface. Increasing particle size shifts the COF range towards lower values (Fig. 4b).

4 Discussion

4.1 Coefficient of Friction

4.1.1 Clean Surface

The COF of a shoe sole on a clean floor surface is primarily composed of viscoelastic and adhesive contributions. The adhesive component is proportional to the real contact area, while the viscoelastic contribution arises from the cyclic deformation of the sole material as the elastomer slides over surface asperities of the floor [22]. The contact area mainly depends on the normal force, the elastic modulus of the contacting materials, and the topography of the contact surfaces [23, 24], but it is also influenced by adhesive forces at the material interface [25]. The viscoelastic contribution is primarily dependent on the sliding velocity, the surface roughness of the hard substrate and the loss tangent of the shoe sole material [26, 27].

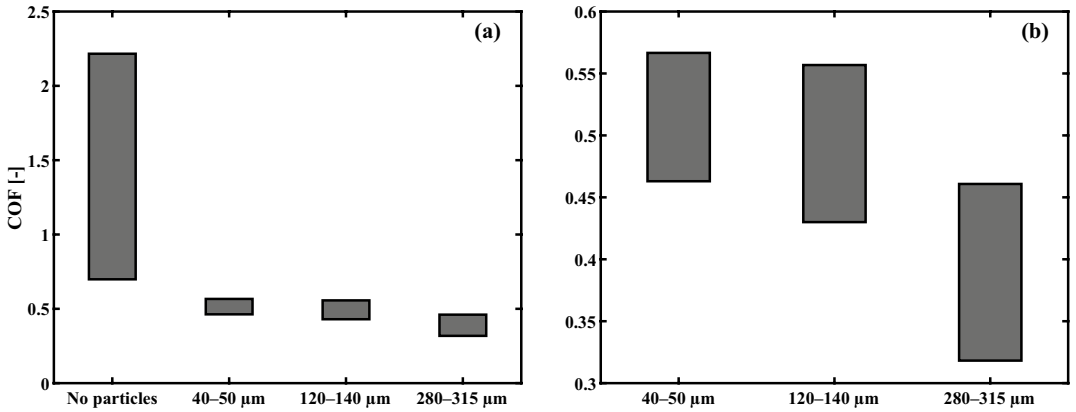

Fig. 4 Ranges of COF reached during the experiments with rubber specimens with varied hardness and surface roughness. All tested surface conditions **a**, particle covered surface conditions **b**

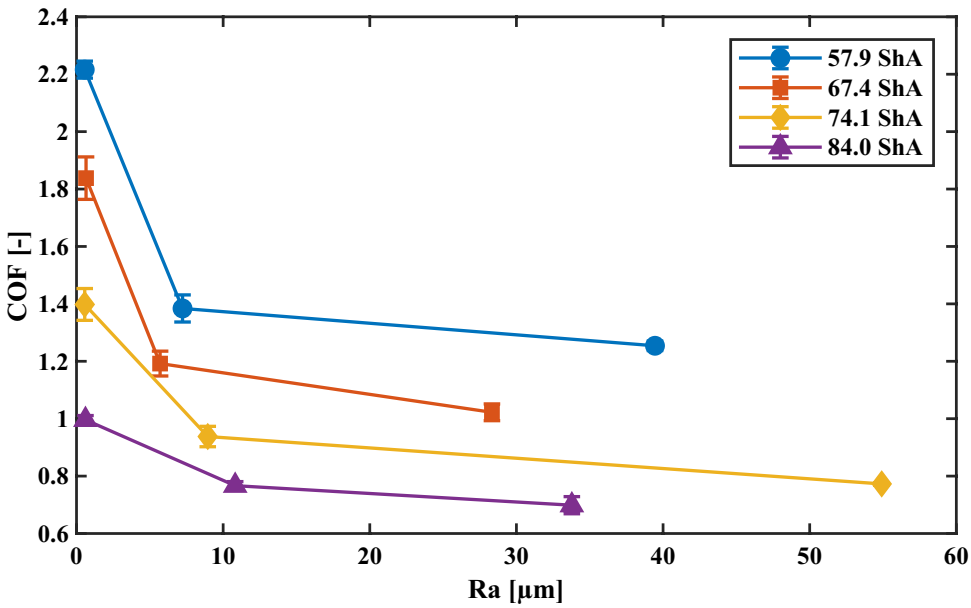

Fig. 5 Effect of rubber surface roughness (Ra) and hardness on the coefficient of friction against a clean epoxy surface

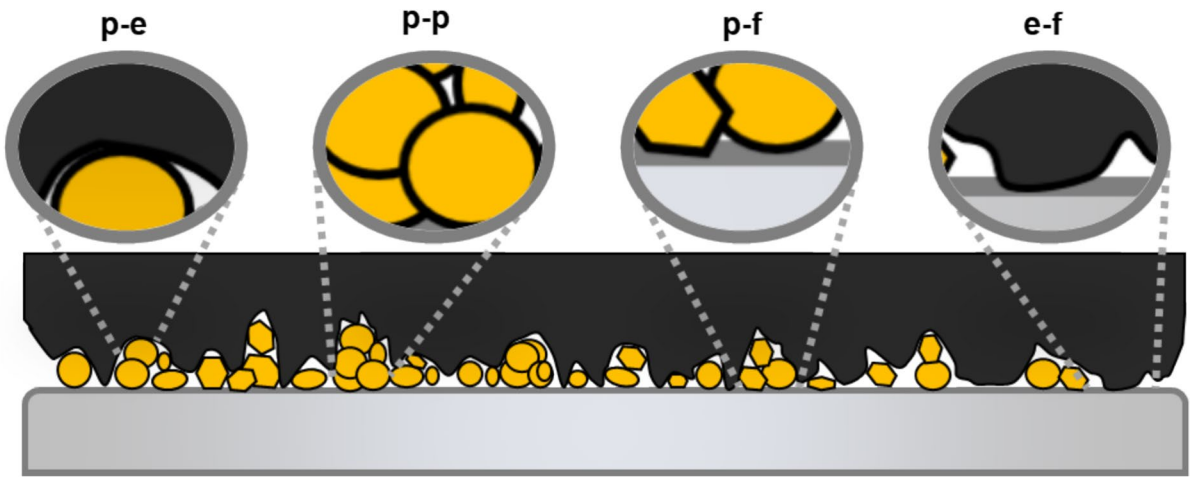

Fig. 6 Schematic representation of interfacial interactions between elastomer, particles, and smooth epoxy floor during sliding

In the case of an NBR rubber–epoxy contact pair, where the epoxy surface is relatively smooth, friction is expected to be governed primarily by adhesion [28]. The COF of rubber sliding against a clean epoxy surface decreases with increasing rubber surface roughness and hardness (Fig. 5). An increase in rubber hardness reduces material deformation under a constant load, thereby decreasing the real contact area and lowering the COF. Similarly, increasing rubber surface roughness also reduces the real contact area, resulting in a further decrease in COF.

4.1.2 Surface Contaminated with Solid Particles

Solid contaminant particles partially hinder direct contact between the shoe sole and the floor, creating a new tribological system (Fig. 6) characterized by four distinct interfaces: particle–elastomer (p–e), particle–floor (p–f), particle–particle (p–p), and elastomer–floor (e–f), each of which can be characterized by a shear strength (τ). Sliding predominantly occurs at the interface with the lowest shear strength [9, 29]. The shear strength at the p–f interface ($\tau_{p\text{-}f}$) increases with the roughness of the contact surface [29]. Particle size and shape also play a significant role. Han et al. [30] found that the shear strength of the sand–steel interface decreases with increasing particle size and roundness. In the case of a smooth epoxy floor, it is expected that sliding will predominantly occur at the p–f interface. Corundum particles are substantially harder than the epoxy surface. During sliding, the epoxy floor undergoes wear in the form of grooving, which contributes to the overall COF in the contact [31].

Vangla et al. [32] studied the shear strength at the interface between sand particles of different size fractions and the surface of a smooth geomembrane (HDPE). Their analysis of surface wear indicated that the COF at the interface between the particle layer and the smooth surface does not depend on particle size, but rather on the number of effective contacts per unit area—those contacts that significantly contribute to surface wear.

The shear strength at the p–p interface (τ_{p-p}) is governed by cohesive forces, friction, and interlocking between particles [33]. With increasing particle size and decreasing roundness, shear strength between layers increases [34]. For larger particles, the effect of interlocking becomes more dominant, while for smaller particles, cohesive forces play a more dominant role [35]. Both Orband et al. [35] and Mills et al. [9] observed a sharp increase in the influence of cohesive forces in particles sized between 50 and 60 µm.

As the majority of the epoxy surface is covered by solid particles, we expect that changes in the surface roughness or hardness of the elastomer primarily affect the direct contact between the elastomer and the particles, and thereby the shear strength of the p–e interface (τ_{p-e}). A rough elastomer surface allows particles to become embedded in its asperities, increasing the shear strength of the p–e interface. This effect has been observed at the interface between solid particles and the floor [9], as well as during the sliding of a layer of calcareous sand over the surface of a steel plate [29]. A decrease in elastomer hardness results in greater deformation under constant load, thereby increasing the real contact area [22]. This increased deformability also facilitates the mechanical interlocking of particles with the sole surface. Consequently, lower hardness and higher surface roughness of the elastomer both contribute to an increase in the shear strength at the p–e interface.

Other authors have also reported an increase in the COF with decreasing elastomer hardness on surfaces

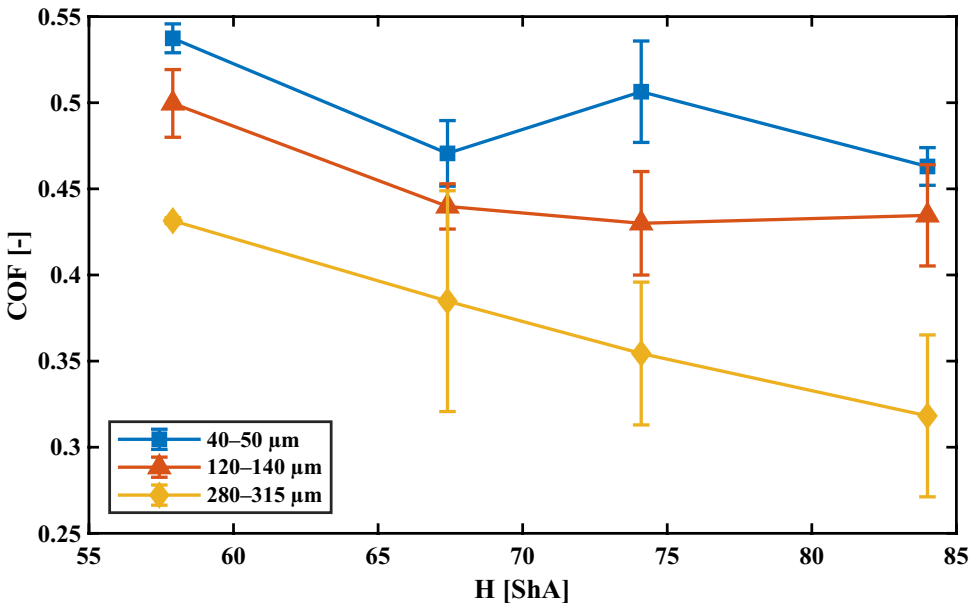

Fig. 7 Dependence of the COF on the hardness of the rubber pin. Only values for smooth rubber surfaces are shown for clarity

contaminated with water [36], oil [37], and even in contact with ice [16]. During sliding of the shoe sole over a floor surface covered with solid particles, direct contact between the elastomer and the floor surface also occurs. This direct contact significantly increases the system's COF, as evidenced by higher COF values observed on clean floor surfaces compared to contaminated ones [38].

4.1.2.1 Effect of Rubber Hardness Rubber hardness has a significant effect on COF ($p < 0.0001$). Higher hardness reduces the COF when larger particles (280–315 µm) are present (Fig. 7). In contrast, smaller particles do not show such a clear trend. For a constant contaminant mass, a greater number of smaller particles are introduced into the contact, effectively forming a more homogeneous layer that limits their ability to roll or tumble [9]. Increasing the rubber hardness primarily reduces the nominal contact area, thereby decreasing the number of particles entrapped within the contact. This reduction in particle population lowers the extent of shearing and inter-particle collisions within the layer. However, a smaller nominal contact area also increases the contact pressure, which in turn promotes the abrasive action of particles grooving the opposing epoxy surface.

Low COF values, combined with dent-like wear patterns on the epoxy surface, suggest that during sliding with a hard sole material, particle motion within the contact zone is predominantly governed by rolling. In contrast, a soft sole material restricts particle mobility at the p-e interface, possibly resulting in a prevailing sliding mechanism. This is consistent with the findings of Rudge et al., who observed higher values of COF in compliant contacts contaminated with smaller particles [18]. The most pronounced decrease in COF is observed for the corundum particle fraction sized 280–315 µm, which exhibits higher roundness compared to the 40–50 µm and 120–140 µm fractions. Softer rubber material creates greater contact area, where particles are pushed against the flooring surface, which leads to formation of more effective contact points at the p-f interface grooving the floor surface. This leads to higher COF values for softer rubber pins. A secondary effect may be the formation of direct rubber-floor contact, which will be greater for softer rubber materials at the constant normal load, also leading to an increase of COF.

4.1.2.2 Effect of Rubber Roughness Rubber roughness also has a significant effect on COF ($p < 0.0001$). With increasing rubber surface roughness, the COF in the particle-contaminated contact increases (Fig. 8). This is consistent with the findings of Xiao et al. [13], who studied particle-contaminated asphalt surfaces of varied roughness. Higher rubber surface roughness promotes the entrapment of particles in the surface valleys, thereby restricting their rolling motion—similarly to the effect of elastomer deformation. Larger surface asperities increase the available free volume for particle entrapment, thereby facilitating direct contact between the rubber and the floor surface.

The influence of rubber surface roughness is more pronounced for the hard elastomer (Fig. 8). Under loading, the highest deformation occurs at the asperities due to locally elevated contact pressures. The asperities of a soft elastomer deform easily, resulting in partial surface levelling and embedding of particles into the elastomer surface. Consequently, the contact scenario resembles that of a smooth soft surface [23], and the COF increases only marginally with increasing rubber surface roughness. In the case of the smooth hard elastomer, particles can roll in the contact, causing low friction. Increasing roughness of a hard elastomer prevents particles from rolling, which leads to an increase in COF. Furthermore, the limited deformability

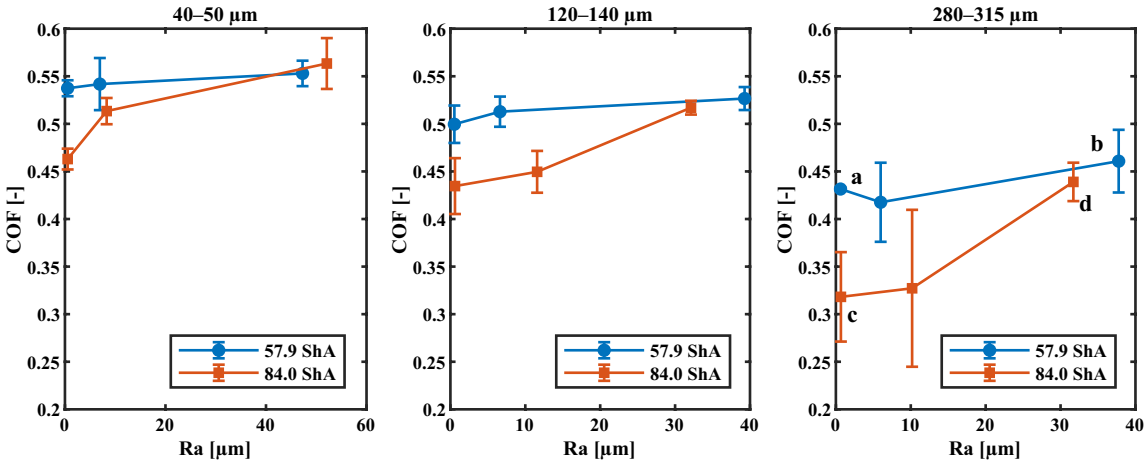

Fig. 8 Dependence of COF on the surface roughness (Ra) of the rubber pin. For clarity, only the values corresponding to the softest and hardest rubber pins are shown. The wear patterns of epoxy surfaces for data points a, b, c, d are displayed in Fig. 10

of asperities in the hard elastomer can cause partial displacement of the particle layer and promote the formation of direct contact between the rubber and the floor, further increasing the COF.

4.1.2.3 Evolution of Friction During Sliding Rubber roughness has a significant effect on the slope of COF during sliding ($p < 0.0001$). An increase in rubber surface roughness leads to a steeper COF slope, as shown in Fig. 9a. During sliding, particles are displaced from the peaks of rubber surface and become firmly embedded in the surface valleys, gradually increasing the number of effective contact points at the p–f interface, and thus, increasing the COF over sliding distance.

Statistical analysis showed that increasing rubber hardness is associated with a slight reduction in the slope ($p = 0.001$); however, the change ($\approx 2 \times 10^{-3}$ mm^{-1} over 57.9–84.0 ShA) is minor relative to the large confidence intervals (Fig. 9b). It was initially expected that the formation of direct contact between the rubber and the flooring surface, and the associated gradual increase in COF, would be more prominent in the case of harder rubber. However, this hypothesis was not supported by the experimental results. A possible explanation is that the asperities of the harder rubber penetrate the particle layer at the initial contact, but during sliding, the influence of direct contact formation becomes overshadowed by other dominant mechanisms occurring at the p–f interface.

4.1.2.4 Particle Size The filling of surface valleys with particles depends not only on the surface roughness of the contacting materials but also on the particle size. Therefore, the effects of surface roughness and particle size on the COF are interrelated [13]. At constant surface roughness and rubber hardness, an increase in particle size results in a decrease in COF. This reduction in COF with increasing contaminant particle size has also been reported by other authors, using various elastomers on both rough and smooth floor surfaces [13, 17, 39].

4.1.2.5 Floor Wear To better understand the phenomena occurring at the interface between the outsole and the floor contaminated with solid particles, the worn surfaces of the epoxy floor were analysed after the COF measurements were performed. All COF measurements were carried out with the same mass of solid particles in the contact. As particle size decreases, the number of particles applied increases, which leads to the formation of more contact points between the particles and the floor surface. At the same time, contact pressure is distributed more evenly across these contact points, which in turn reduces the depth of surface grooves at individual contact points, as this depth is dependent on the applied normal load [31].

A comparison of floor surface wear for identical particle size fractions of the contaminant shows that the COF increases proportionally with surface wear (Fig. 10a–d). Almost no longitudinal grooves are observed on the epoxy surface after sliding with hard smooth rubber (Fig. 10c). Most of the wear appears as dents, indicating that particle rolling plays a dominant role in the contact between the rubber and the floor. On the epoxy surface after sliding with soft smooth rubber (Fig. 10a), generally higher wear is observed, with a greater proportion of longitudinal grooves.

High surface roughness of the rubber pin facilitates embedding of particles into surface valleys. This may enhance the shear strength at the p–e interface, causing particles to be dragged along with the elastomer during sliding. As a result, a large number of longitudinal grooves are formed on the epoxy surface, even when hard rubber is used (Fig. 10d). Nevertheless, localized rolling of particles may

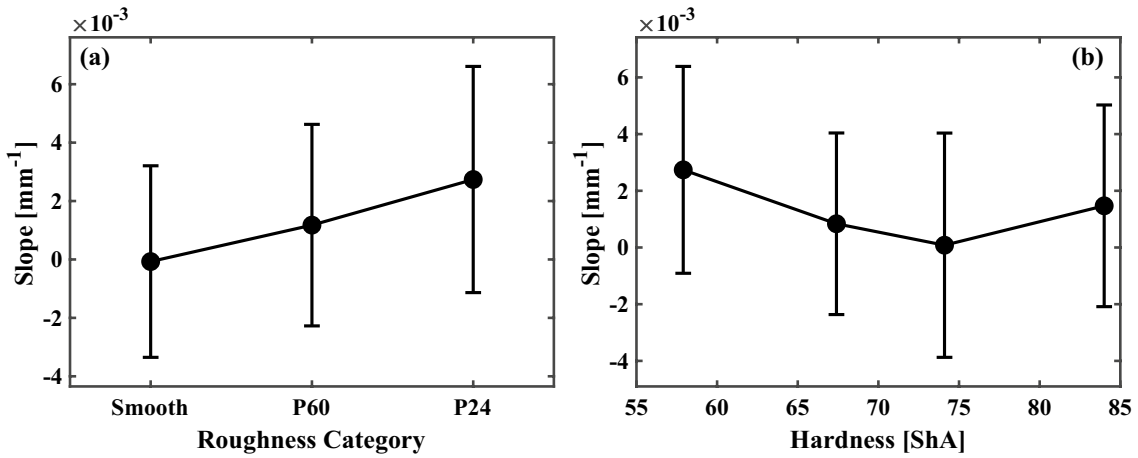

Fig. 9 Slope of COF and standard deviation for all particle-contaminated conditions categorized by rubber surface roughness **a** and hardness **b**

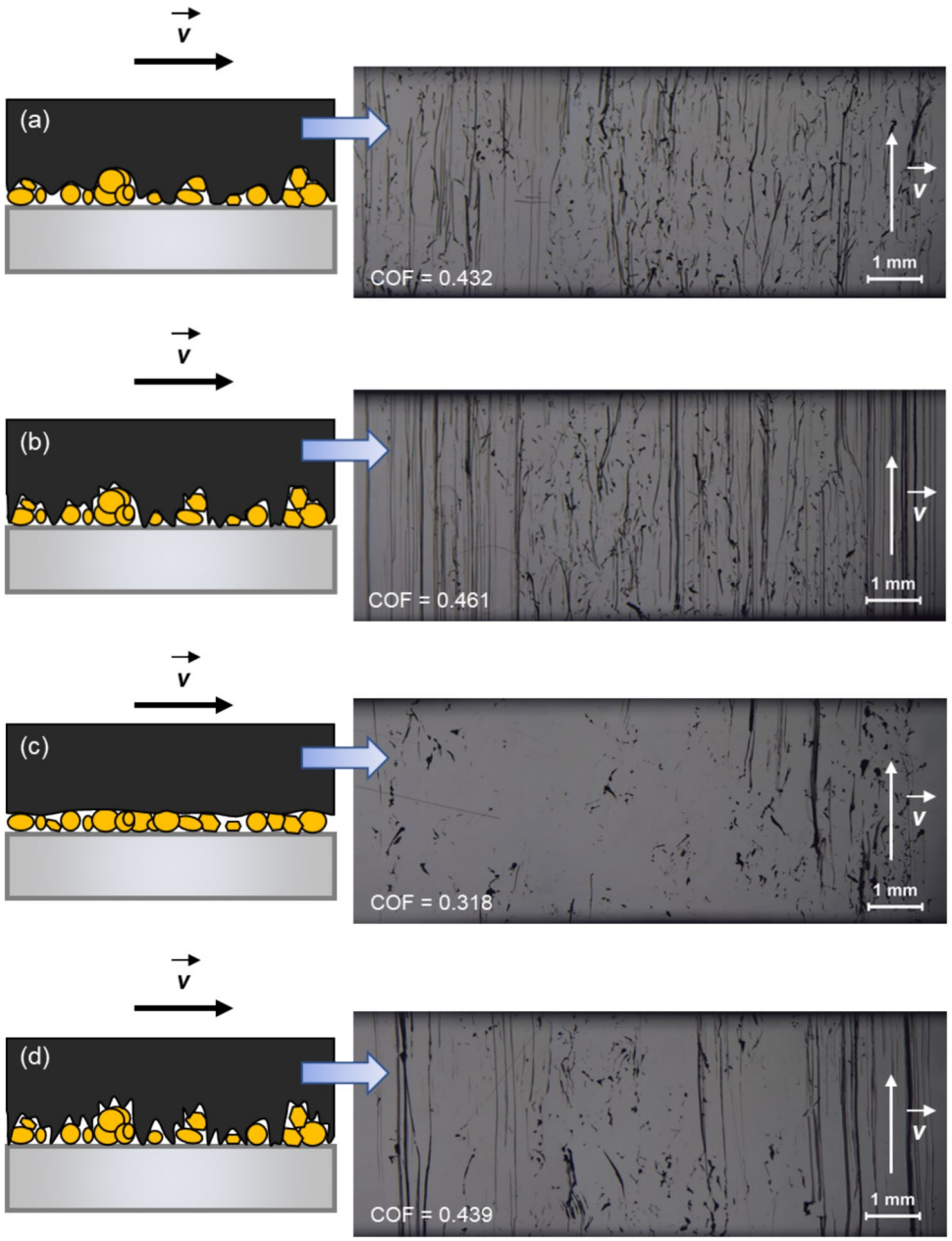

Fig. 10 Schematic illustrations (left), based on friction trends and surface wear analysis, proposing possible contact configurations between rubber specimens of varied hardness and surface roughness sliding over a particle-contaminated epoxy floor. The corresponding wear tracks (right) on the epoxy floor after experiments using: **a** soft smooth rubber, **b** soft rough rubber, **c** hard smooth rubber, and **d** hard rough rubber. Particle size fraction: 280–315 µm. Direction of sliding indicated by arrows. COF values represent the average coefficient of friction measured during the test

still occur. After sliding with soft rubber of high surface roughness, the worn epoxy surface displays a clear dominance of long scratches (Fig. 10b), indicating that most of the particles in contact were firmly entrapped in the rubber surface.

Most of the variability in COF values measured in contacts between rubber pins of different hardness and surface roughness and the smooth epoxy floor can be explained by the nature of the floor surface wear. Higher COF values that are disproportionate to the extent of epoxy surface wear can be explained by direct contact between the rubber and the epoxy. For the particle size fraction of 40–50 µm, the highest COF value was observed with the hard rubber pin with high surface roughness (H = 84.0 ShA, Ra = 52.1 µm). The asperities on the rough surface of the hard rubber may displace the layer of small particles and establish direct contact with the epoxy floor right after the initial contact. A portion of the load is then transmitted through direct contact between the rubber and the floor, leading to an increase in the COF without an associated increase in epoxy surface wear.

5 Limitations and Future Outlook

Although the present study provides valuable insights into the influence of elastomer hardness and surface roughness on friction in particle-contaminated shoe–floor contacts, several limitations should be acknowledged.

The effects of rubber hardness and surface roughness were investigated using a laboratory tribometer (pin-on-plate configuration), which allows precise control of normal force, sliding velocity, and surface conditions. The COF measurement protocol was designed to approximate conditions at heel-strike during normal walking. However, it does not fully capture the complex biomechanics of human gait or the geometry of real footwear. Future studies should validate the observed frictional mechanisms using full-scale tests with whole-shoe tribometers to incorporate the effects of footwear geometry, loading patterns, and gait dynamics in realistic slip scenarios.

The mechanisms of sliding between the rubber sole and the floor in the presence of particles were inferred from COF values and surface wear patterns. However, particle motion within the contact zone was not directly observed. In situ monitoring of the real contact area, or the use of contact visualization techniques, could provide a more detailed understanding of interfacial behaviour under particle-contaminated conditions.

Furthermore, the study focused on a smooth floor surface uniformly covered with hard particles. In contrast, real-world environments often involve partial contamination and a broader range of particulate types, including soft or adhesive materials such as sand or clay. Extending the scope to include different contaminant properties and coverage levels would enhance the generalizability of the findings.

Lastly, the study did not address the adherence of particles to the shoe sole, which may influence friction even after the contaminated surface has been left. Future research should explore how material hardness and roughness affect particle retention and transport on the outsole.

Despite these limitations, the results offer a robust foundation for optimizing elastomer properties in the design of footwear intended for use in particle-contaminated environments.

6 Conclusion

This study investigated the influence of elastomer hardness and surface roughness on the frictional behaviour of shoe soles sliding over smooth floor surfaces contaminated with solid particles. Experiments were conducted using a pin-on-plate tribometer simulating heel-strike conditions during walking. The COF was measured for various combinations of rubber hardness, rubber surface roughness, and particle size. The primary objective was to understand how sole material properties affect interaction with particle-contaminated floors. The key findings are summarized as follows:

- On a clean epoxy surface, an increase in both rubber hardness and surface roughness resulted in a decrease in COF, primarily due to a reduction in real contact area and adhesive interactions. The reduction in COF associated with changes in rubber properties was substantially greater on clean surfaces than on contaminated ones, as the majority of slip in the latter occurs at the particle–floor interface, which is primarily governed by the properties of the particles and floor material. In such cases, sole material properties play only a secondary role.
- Under particle-contaminated conditions, the opposite trend was observed: COF increased with increasing rubber roughness, particularly for harder elastomers. Higher rubber surface roughness was associated with increased epoxy wear and the formation of longitudinal grooves, suggesting that rough rubber promotes particle entrapment and dragging, whereas smooth rubber enables particles to roll within the contact, leading to lower COF.
- Increased roughness also resulted in a steeper COF slope during sliding, indicating a more dynamic evolution of friction. This was attributed to the formation of direct contact between rubber asperities and the floor as particles were displaced from the interface.
- On particle-contaminated surfaces, increasing rubber hardness led to a reduction in COF.
- Particle shape and size also had a significant effect on the COF between rubber and a particle-contaminated surface ($p < 0.0001$). COF decreased with increasing particle size, with the most pronounced reduction observed for the size fraction 280–315 μm, which also exhibited the highest roundness.

In summary, this study confirms that both elastomer hardness and surface roughness play important roles in determining frictional behaviour on both clean and particle-contaminated surfaces. On smooth flooring materials such as epoxy-coated floor, slip predominantly occurs at the particle–floor interface. In contaminated contacts, the frictional response is governed by the competition between particle rolling, sliding, and direct rubber–floor contact. Based on post-test observations of wear patterns and analysis of COF, we infer that rubber hardness and surface roughness primarily influence the strength of the particle–elastomer interface. A stronger p–e interface suppresses particle rolling, which in turn leads to higher COF values.

These findings are relevant for optimizing outsole design in footwear intended for use in particle-contaminated

environments, including industrial workplaces, construction sites, and outdoor settings.

Author Contributions M.Ž. and D.M. conceived the idea. M. Ž. and D. R. designed the experiments. M. Ž. and D. M. performed the experiments and analysed the data. M. Ž., D. R., and D. M. wrote the original draft of the manuscript. M. V., M. H., and L. K. administrated the project, secured funding, and supervised the study.

Funding Open access publishing supported by the institutions participating in the CzechELib Transformative Agreement. This study was supported by the internal grant of the Brno University of Technology focused on specific research and development No. FCH/FSI-J-24–8561 and also supported by the project "Mechanical Engineering of Biological and Bio-inspired Systems", funded as Project No. CZ.02.01.01/00/22_008/0004634 by Programme Johannes Amos Comenius, call Excellent Research, administered by the Ministry of Education, Sports and Youth.

Data Availability The data that support the findings of this study are openly available in repository Zenodo at https://doi.org/10.5281/zenodo.15410868.

Declarations

Conflict of interest The authors declare no competing interests.

References

1. Health and safety executive. Non-fatal injuries at work in Great Britain 2024. https://www.hse.gov.uk/statistics/causinj/index.htm (Accessed 1 Feb 2025).
2. Ohnishi, A.: Causes of occupational falls on the same level more than four days absence from work: the Japanese. J. Ergon. **56**, 101–107 (2020). https://doi.org/10.5100/jje.56.101
3. U.S. Bureau of Labor Statistics. Injuries, Illnesses, and Fatalities 2021. https://www.bls.gov/iif/nonfatal-injuries-and-illnesses-tables/case-and-demographic-characteristics-table-r4-2020.htm (Accessed 12 April 2024).
4. Courtney, T.K., Sorock, G.S., Manning, D.P., Collins, J.W., Holbein-Jenny, M.A.: Occupational slip, trip, and fall-related injuries - Can the contribution of slipperiness be isolated? Ergonomics **44**, 1118–1137 (2001). https://doi.org/10.1080/00140130110085538
5. Strobel, C.M., Menezes, P.L., Lovell, M.R., Beschorner, K.E.: Analysis of the contribution of adhesion and hysteresis to shoe-floor lubricated friction in the boundary lubrication regime. Tribol. Lett. **47**, 341–347 (2012). https://doi.org/10.1007/s11249-012-9989-5
6. Redfern, M.S., Cham, R., Gielo-Perczak, K., Grönqvist, R., Hirvonen, M., Lanshammar, H., et al.: Biomechanics of slips. Ergonomics **44**, 1138–1166 (2001). https://doi.org/10.1080/00140130110085547
7. Moore, C.T., Menezes, P.L., Lovell, M.R., Beschorner, K.E.: Analysis of shoe friction during sliding against floor material: role of fluid contaminant. J. Tribol. (2012). https://doi.org/10.1115/1.4007346
8. Li, K.W., Hsu, Y.-W., Chang, W.-R., Lin, C.-H.: Friction measurements on three commonly used floors on a college campus under dry, wet, and sand-covered conditions. Saf. Sci. **45**, 980–992 (2007). https://doi.org/10.1016/j.ssci.2006.08.030
9. Mills, R., Dwyer-Joyce, R.S., Loo-Morrey, M.: The mechanisms of pedestrian slip on flooring contaminated with solid particles. Tribol. Int. **42**, 403–412 (2009). https://doi.org/10.1016/j.triboint.2008.07.013
10. Xue, Y., Li, P., Zhao, C., Wang, Y., Sun, C., Khan, M.D.: Investigation to the skid resistance of asphalt pavement based on the movement of aeolian sand. Constr. Build. Mater. **318**, 125986 (2022). https://doi.org/10.1016/J.CONBUILDMAT.2021.125986
11. Hichri, Y., Cerezo, V., Do, M.T., Zahouani, H.: Effect of particles' characteristics and road surface's texture on the tire/road friction. Surf. Topogr. **6**, 034014 (2018). https://doi.org/10.1088/2051-672X/aad063
12. Changarnier, S., Hichri, Y., Cerezo, V., Do, M.-T., Salvatore, F., Zahouani, H.: Observations of dry particles behaviour at the tyre/road interface. Tribol. Int. **128**, 291–301 (2018). https://doi.org/10.1016/j.triboint.2018.07.023
13. Xiao, S., Xi, C., Xu, L., Li, J., Tan, Y.: Effects of road particulate contaminants on pavement skid resistance. Road Mater. Pavement Design **25**, 874–887 (2024). https://doi.org/10.1080/14680629.2023.2229921
14. Chang, W.-R.: The effect of surface roughness and contaminant on the dynamic friction of porcelain tile. Appl. Ergon. **32**, 173 (2001)
15. Chang, W.-R.: The effects of surface roughness and contaminants on the dynamic friction between porcelain tile and vulcanized rubber. Saf. Sci. **40**, 577–591 (2002). https://doi.org/10.1016/S0925-7535(01)00060-1
16. Isitman, N.A., Kriston, A., Fülöp, T.: Role of rubber stiffness and surface roughness in the tribological performance on ice. Tribol. Trans. **61**, 295–303 (2018). https://doi.org/10.1080/10402004.2017.1319002
17. Li, K.W., Meng, F., Zhang, W.: Friction between footwear and floor covered with solid particles under dry and wet conditions. Int. J. Occup. Saf. Ergon. **20**, 43–53 (2014). https://doi.org/10.1080/10803548.2014.11077027
18. Rudge, R.E.D., Theunissen, K., Stokes, J.R., Scholten, E., Dijksman, J.A.: Tribology of hard particles lubricating soft surfaces. Phys. Rev. Mater. **5**, 055604 (2021). https://doi.org/10.1103/PhysRevMaterials.5.055604
19. International Organization for Standardization. Plastics and ebonite — Determination of indentation hardness by means of a durometer (Shore hardness) 2003.
20. Chang, W.R., Grönqvist, R., Leclercq, S., Myung, R., Makkonen, L., Strandberg, L., et al.: The role of friction in the measurement of slipperiness, Part 1: Friction mechanisms and definition of test conditions. Ergonomics **44**, 1217–1232 (2001). https://doi.org/10.1080/00140130110085574
21. Redfern, M.S., Rhoades, T.P.: Fall Prevention in Industry Using Slip Resistance Testing. In: Bhattacharya, A., McGlothlin, J.D. (eds.) Occupational Ergonomics Theory and Applications, pp. 463–476. Marcel Dekker, Inc., New York (1996)
22. Tiwari, A., Miyashita, N., Espallargas, N., Persson, B.N.J.: Rubber friction: The contribution from the area of real contact. J. Chem. Phys. (2018). https://doi.org/10.1063/1.5037136

23. Tiwari, A., Persson, B.N.J.: Cylinder-flat contact mechanics with surface roughness. Tribol. Lett. (2021). https://doi.org/10.1007/s11249-020-01380-z
24. Maegawa, S., Itoigawa, F., Nakamura, T.: Effect of normal load on friction coefficient for sliding contact between rough rubber surface and rigid smooth plane. Tribol. Int. **92**, 335–343 (2015). https://doi.org/10.1016/j.triboint.2015.07.014
25. Persson, B.N.J.: Silicone rubber adhesion and sliding friction. Tribol. Lett. **62**, 34 (2016). https://doi.org/10.1007/s11249-016-0680-0
26. Heinrich, G., Klüppel, M., Vilgis, T.A.: Evaluation of self-affine surfaces and their implication for frictional dynamics as illustrated with a Rouse material. Comput. Theor. Polym. Sci. **10**, 53–61 (2000). https://doi.org/10.1016/S1089-3156(99)00033-1
27. Persson, B.N.J.: Theory of rubber friction and contact mechanics. J. Chem. Phys. **115**, 3840–3861 (2001). https://doi.org/10.1063/1.1388626
28. Pinnington, R.J.: Rubber friction on rough and smooth surfaces. Wear **267**, 1653–1664 (2009). https://doi.org/10.1016/j.wear.2009.06.011
29. Lei, K.H., Zhou, D.W., Chun, Z.W., Bin, Z.J., Ni, P., Ba, J., et al.: Experimental study of interface shearing between calcareous sand and steel plate considering surface roughness and particle size. Appl. Ocean Res. **107**, 102490 (2021). https://doi.org/10.1016/J.APOR.2020.102490
30. Han, F., Ganju, E., Salgado, R., Prezzi, M.: Effects of interface roughness, particle geometry, and gradation on the sand-steel interface friction angle. J. Geotech. Geoenv. Eng. (2018). https://doi.org/10.1061/(ASCE)GT.1943-5606.0001990
31. Walker, J., Umer, J., Mohammadpour, M., Theodossiades, S., Bewsher, S.R., Offner, G., et al.: Asperity level characterization of abrasive wear using atomic force microscopy. Proc. Royal Soc. A: Math. Phys. Eng. Sci. (2021). https://doi.org/10.1098/rspa.2021.0103
32. Vangla, P., Latha, G.M.: Influence of particle size on the friction and interfacial shear strength of sands of similar morphology. Int. J. Geosynth. Ground Eng. (2015). https://doi.org/10.1007/s40891-014-0008-9
33. Shi, H., Mohanty, R., Chakravarty, S., Cabiscol, R., Morgeneyer, M., Zetzener, H., et al.: Effect of particle size and cohesion on powder yielding and flow. KONA Powder Part. J. **2018**, 226–250 (2018). https://doi.org/10.14356/kona.2018014
34. Liu, T., Wang, X., Ally, H., Wu, T.: Effect of particle size and two-dimensional shape on internal friction angle of dry sand using image processing. Adv. Powder Technol. (2024). https://doi.org/10.1016/j.apt.2024.104467
35. Orband, J.L.R., Geldart, D.: Direct measurement of powder cohesion using a torsional device. Powder Technol. **92**, 25–33 (1997). https://doi.org/10.1016/S0032-5910(97)03212-9
36. Ishizako, A., Nishi, T., Yamaguchi, T.: Effect of orientation and hardness of rubber tread block on the friction coefficient under glycerol lubrication and its underlying mechanisms. Tribol. Int. (2024). https://doi.org/10.1016/j.triboint.2024.109904
37. Iraqi, A., Vidic, N.S., Redfern, M.S., Beschorner, K.E.: Prediction of coefficient of friction based on footwear outsole features. Appl. Ergon. (2020). https://doi.org/10.1016/j.apergo.2019.102963
38. Jakobsen, L., Lysdal, F.G., Bagehorn, T., Kersting, U.G., Sivebaek, I.M.: The effect of footwear outsole material on slip resistance on dry and contaminated surfaces with geometrically controlled outsoles. Ergonomics **66**, 322–329 (2023). https://doi.org/10.1080/00140139.2022.2081364
39. Hichri, Y., Descartes, S., Cerezo, V., Do, M.T.: Understanding the behavior of fine particles at the tire/road interface. Tribol. Int. (2020). https://doi.org/10.1016/j.triboint.2019.02.043